Nonlinear Electrophoresis of Colloids Controlled by Anisotropic Conductivity and Permittivity of Liquid-Crystalline Electrolyte

Sathyanarayana Paladugu, Christopher Conklin, Jorge Viñals, and Oleg D. Lavrentovich

Phys. Rev. Applied **7**, 034033 — Published 30 March 2017

DOI: 10.1103/PhysRevApplied.7.034033

Nonlinear electrophoresis of colloids controlled by anisotropy of conductivity and permittivity of liquid crystal electrolyte

Sathyanarayana Paladugu[1], Christopher Conklin[2], Jorge Viñals[2], and Oleg D. Lavrentovich[1†]

[1]Liquid Crystal Institute and Chemical Physics Interdisciplinary Program,

Kent State University, Kent, OH 44242

[2]School of Physics and Astronomy,

University of Minnesota, Minneapolis, MN 55455

Abstract

Liquid crystal electrolytes enable nonlinear electrophoresis of colloidal particles with velocities proportional to the square of the applied field. We demonstrate that the magnitude and even the polarity of electrophoretic mobility can be controlled by the anisotropy of electric conductivity and dielectric permittivity of the liquid crystal. In particular, reversal of electrophoretic mobility can be triggered either by temperature or composition changes that alter the signs of the conductivity and permittivity anisotropies. Controllable reversal of mobility adds to the list of advantages of anisotropic electrolytes over their isotropic counterparts.

† olavrent@kent.edu

INTRODUCTION

Microscale manipulation of colloidal particles and fluids by electric fields is a broad area of active scientific research ranging from fundamental studies of non-equilibrium phenomena [1-4] to the development of practical devices for informational displays, portable diagnostics, sensing, delivery, and sorting [5-7]. It has been demonstrated recently [4,8-10] that when a nematic liquid crystal is used as an electrolyte instead of an isotropic fluid, electrokinetic phenomena acquire qualitatively new characteristics. An important feature of the nematic electrolyte is that the space charge is generated in the medium, at the distortions of molecular orientations, rather than at the interface between the particle and the electrolyte. Space charge separation occurs in the applied electric field, which drives positive and negative ions to different regions of the deformed liquid crystal thanks to the anisotropy of conductivity and dielectric permittivity [8-10]. The electric field then imposes an electrostatic force on the charged clouds, setting the nematic into electrokinetic flows with the velocities growing as the square of the applied field E (one degree of E separates the charges, the other drives the flows) [8-10]. The quadratic dependence means that the electrophoretic and electro-osmotic velocities do not depend on the polarity of the applied electric field. This feature brings an important advantage of the liquid crystal-enabled electrokinetics (LCEK) over its isotropic linear counterpart since one can use an alternating current (AC) electric field as a driving force to cause a unidirectional persistent motion of particles or of the liquid crystal with a steady displacement that remains nonzero after averaging over the period of the AC field [9,11]. Furthermore, orientational order of the electrolyte allows one to design trajectories

of the colloids by patterning the director $\hat{\boldsymbol{n}}$ that specifies local orientation of the liquid crystal [8,11].

Theoretically, the electrokinetic velocities are expected to depend on the type of director distortions in the liquid crystal and on the anisotropy [8-10]. In this work, we consider one of the simplest realizations of LCEK, namely, a liquid crystal-enabled electrophoresis (LCEP) of a sphere of a radius R with perpendicular surface anchoring. When placed in a uniformly aligned nematic cell, with the director aligned, say, along the x-axis of the Cartesian coordinate system, $\hat{\boldsymbol{n}}_0 = (1,0,0)$, Figure *1*, such a sphere distorts the director around itself because of the finite strength of surface anchoring. These distortions, being radial near the sphere, need to match the far-field uniform director $\hat{\boldsymbol{n}}_0$. The matching is achieved through the introduction of a point defect, the so-called hyperbolic hedgehog that can be located either on the left side or the right side of the sphere, Figure 1 [12]. Once formed, the hyperbolic hedgehog does not change sides since the energy barrier is orders of magnitude higher than the thermal energy. It also does not change sides when the sample is acted upon by electric fields of a modest amplitude used in this work. The overall director structure of the hedgehog-sphere pair is of the dipolar type. We direct the structural dipole $\boldsymbol{p} = (p,0,0)$ from the hedgehog towards the sphere, along the *x*-axis, Figure 1b. When the hedgehog is located on the left hand side of the sphere, $p > 0$, the experimental mapping of the material flow around the sphere placed in a liquid crystal with zero dielectric anisotropy suggests that the electrophoretic velocity

$\boldsymbol{v} = (v, 0, 0)$ is antiparallel to the direction of dipole, $v < 0$ [9]. Theoretically, the amplitude of electrophoretic velocity is predicted to be [9]

$$v = \alpha \varepsilon_0 \varepsilon_\perp \eta_{||}^{-1} (\tilde{\varepsilon} - \tilde{\sigma}) RE^2, \quad (1)$$

where ε_0 is permittivity in vacuum, $\eta_{||}$ is the effective nematic viscosity, $\tilde{\varepsilon} = \varepsilon_{||} / \varepsilon_\perp - 1$ is anisotropy of permittivity and $\tilde{\sigma} = \sigma_{||} / \sigma_\perp - 1$ is anisotropy of conductivity; the subscripts $||$ and $\perp$ refer to the orientation parallel and perpendicular to $\hat{\boldsymbol{n}}$, respectively, and α is a numerical parameter of the order of 1 that should depend on the details of director configuration, finite surface anchoring, anisotropy of viscoelastic parameters of the nematic; its exact theoretical value is not known. Although the experiments support the model in the part of $v \propto RE^2$ dependence [8,9,11,13-15] and in the guiding effect of the director field [8,11,16-19], there are no experimental data on how v depends on $\tilde{\varepsilon}$ and $\tilde{\sigma}$, the two crucial properties of the nematic electrolyte. As predicted by Eq.(1), one can reverse the direction of velocity $\boldsymbol{v}$ with respect to the structural dipole $\boldsymbol{p}$ by altering the sign of $(\tilde{\varepsilon} - \tilde{\sigma})$. When $(\tilde{\varepsilon} - \tilde{\sigma}) > 0$, the electrophoretic velocity is parallel to the structural dipole; this case is illustrated in Figure *1*; when $(\tilde{\varepsilon} - \tilde{\sigma}) < 0$, the two vectors are antiparallel. Flow reversals have been observed in isotropic electrolytes but their mechanisms are not fully understood [1]. In the present work, we design experiments to verify the key element of LCEK mechanism, by using nematics with broadly varying $\tilde{\varepsilon}$ and values of $(\tilde{\varepsilon} - \tilde{\sigma})$ that reverse their sign as a function of temperature. We

demonstrate that $v \propto (\tilde{\varepsilon} - \tilde{\sigma})$, as predicted by Eq.(1), and can reverse its sign as a function of composition and temperature.

EXPERIMENTAL RESULTS

Materials. We used binary mixtures of room-temperature nematics pentylcyanobiphenyl (5CB) and HNG715600-100 (purchased from Jiangsu Hecheng Display Technology and referred to as HNG in what follows). 5CB exhibits $\tilde{\varepsilon} = 1.9$ [20] and HNG exhibits $\tilde{\varepsilon} = -0.7$ [21] at room temperature. Concentration variation of mixtures changes $(\tilde{\varepsilon} - \tilde{\sigma})$ strongly, both in absolute value and in sign. Dry soda-lime-silica spheres of diameter $2R = (9.6 \pm 1)\ \mu m$ (purchased from ThermoScientific) were used as electrophoretic particles. The spheres were treated with dimethyloctadecyl[3-(trimethoxysilyl)propyl]ammonium chloride (DMOAP) to impart perpendicular orientation of $\hat{\boldsymbol{n}}$. The nematic layers of thickness $h = 60\ \mu m$ were confined between two glass plates with planar alignment, $\hat{\boldsymbol{n}}_0 = (1, 0, 0)$, achieved by rubbed polymer coating (PI-2555, purchased from HD Microsystems). The temperature was controlled by Linkam controller TMS94 and a hot stage LTS350 (Linkam Scientific Instruments) with accuracy $\pm 0.01\,^{\circ}C$.

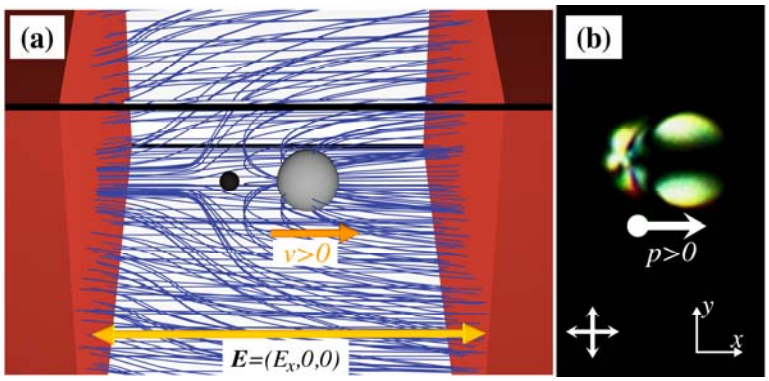

Figure 1. (a) Scheme of electrophoresis for the case $(\tilde{\varepsilon}-\tilde{\sigma})>0$; (b) microphotograph of a glass sphere with a point defect "hedgehog" (located on the left) placed in the nematic liquid crystal, seen between cross polarizers. The structural dipole $\boldsymbol{p}=(p,0,0)$ is shown by an arrow.

Electric field distribution in the cell. The AC voltage of frequency $f=25$ Hz and amplitude $U=100\ V$ was applied between two aluminum strips separated by a distance $L=4\ mm$, Figure 1 and Figure *2*a. The electric field at the center of the nematic slab is smaller than the applied field because of the difference in dielectric permittivities of glass and nematic [9]. The electric field distribution within the cell was determined using finite-element modeling simulator, COMSOL multiphysics, Figure 2b. In electric field simulations, we used the following experimental parameters: distance between the electrodes $L=4\ mm$, cell thickness $h=60\ \mu m$, dielectric permittivity of glass equals 3.9 and average dielectric permittivity of the liquid crystal equals 16. At the center of cell, the field is uniform; it is parallel to the glass plates, but its amplitude is somewhat smaller than the amplitude of the applied field, $E=\beta U/L$, where U is the applied voltage and the correction factor $\beta<1$. For the geometry used in electrophoretic experiments, we

find $\beta = 0.79$ in the center of the nematic slab, Figure 2c. Hence, the field acting on the particles in the center of the cells is $E = 19.75\, mV/\mu m$ which is 79% of the applied field.

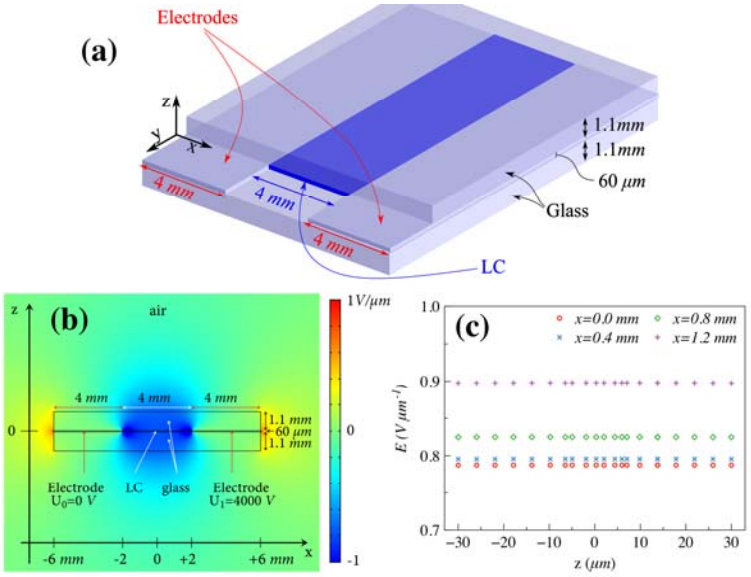

Figure 2 (a) Schematic diagram of the experimental cell; (b) electric field distribution in the plane of the nematic slab and (c) electric field at different locations (x, z) within the nematic slab; the point (0,0) corresponds to the geometrical center of the slab.

Reversal of electrophoretic velocity *v* by composition. We designed the experiments in such a way that $\tilde{\varepsilon}$ varied broadly from mixture to mixture while the anisotropy of conductivity remained constant, $\tilde{\sigma} = 0.4$. To achieve these conditions, the experiments were performed at the temperature $t = T - T_{NI} = -5\,^{\circ}C$ for each mixture, where T_{NI} is the temperature of the isotropic-nematic transition of that mixture, Figure 3a. At high weight concentrations of 5CB, $c > 0.54$, the spheres move with the sphere

leading the way, $v>0$, Figure 3b. For $c<0.54$, the polarity is reversed, $v<0$, i.e., the sphere follows the hedgehog, Figure 3b.

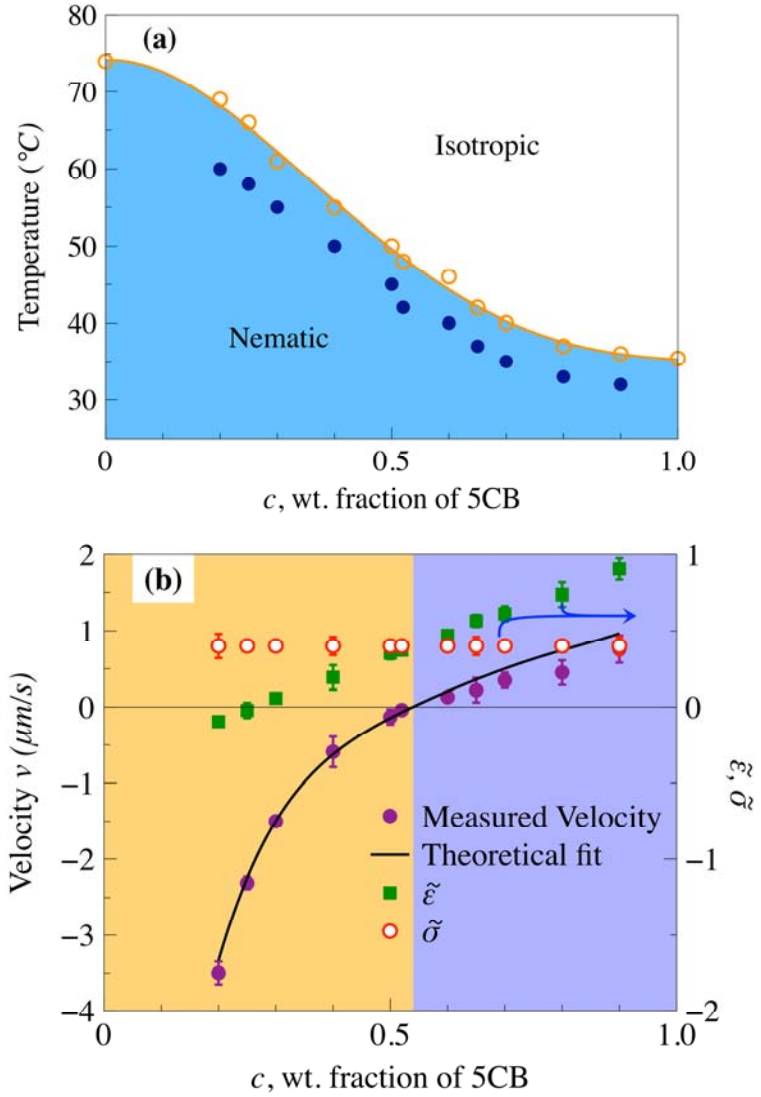

Figure 3. (a) Phase diagram of 5CB-HNG mixtures. Open circles show T_{NI} and the filled circles show the temperatures $t=T-T_{NI}=-5\,^{\circ}C$ at which the material parameters and electrophoretic velocities were measured; (b) Concentration dependence of electrophoretic velocity v, dielectric $\tilde{\varepsilon}$ and conductivity $\tilde{\sigma}$ anisotropies; solid line is the fit of $v(c)$ by Eq. (1) with $\alpha=1.1\pm0.2$.

Reversal of electrophoretic velocity v by temperature change. Analysis of the data in Figure 3 suggests that the polarity of electrophoresis can be reversed by simply changing the temperature of the nematic mixture with concentrations close to $c = 0.52$. Figure 4 shows that this is indeed the case, as the electrophoretic velocity changes from negative to positive as the temperature decreased, with $t_v \approx -7\,°C$ being the point of reversal.

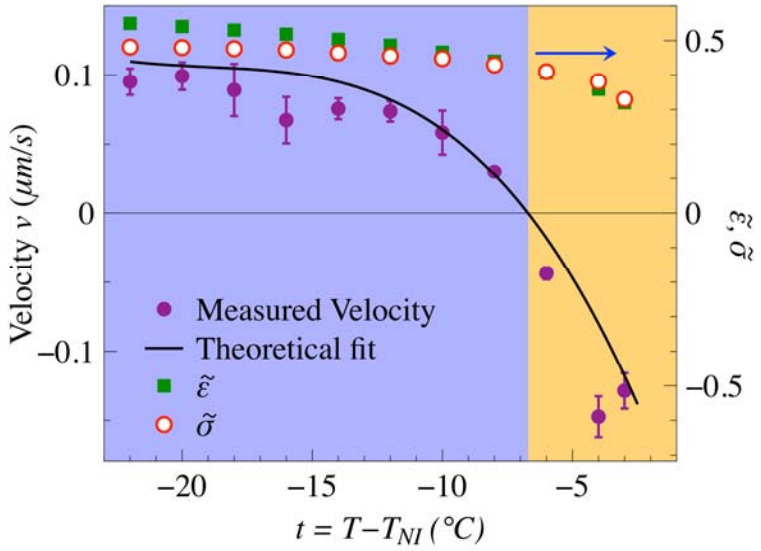

Figure 4. Temperature-triggered reversal of electrophoretic velocity v, plotted together with the temperature dependencies of $\tilde{\varepsilon}$, and $\tilde{\sigma}$ for a binary mixture $c = 0.52$; the solid line is the fit of $v(t)$ by Eq.(1), with $\alpha = 1.2 \pm 0.2$.

To understand the physical reason for the velocity reversal, we performed a thorough characterization of the material properties entering Eq.(1), as described below.

Anisotropy of electric conductivity. The conductivity of nematics is of an ionic type [22,23]. Ions are always present in liquid crystals, representing synthetic impurities, or being produced at electrodes, through dissociation of neutral molecules, absorption from surroundings such as glue, alignment layers, etc.[23]. We measured the concentration using the transient current technique and determined it to be on the order of $10^{20}\ m^{-3}$. To determine $\sigma_{\|}/\sigma_{\perp}$, we tracked transient currents in cells of thickness $15\ \mu m$ with homeotropic and planar alignment, in response to a square wave voltage of frequency 1 Hz and amplitude $(4-7)\ V$ [24]. The ratio of times required by the ions to migrate through the cell determines the ratio of ionic mobilities, which in its turn, yields $\sigma_{\|}/\sigma_{\perp}$ and thus $\tilde{\sigma}$. We find $\tilde{\sigma} \approx 0.4$ for all mixtures at $t = -5\ ^{\circ}C$, Figure 3b.

Dielectric anisotropy. The complex dielectric constants $\varepsilon^*(\omega) = \varepsilon'(\omega) - j\varepsilon''(\omega)$, where $j = \sqrt{-1}$, $\varepsilon'(\omega)$, $\varepsilon''(\omega)$ are real and imaginary parts of complex dielectric constants, and $\omega = 2\pi f$ is angular frequency, were measured for a frequency range of $f = 10\ \text{Hz} - 1\ \text{MHz}$ using Solatron 1260 impedance analyzer and nematic cells with homeotropic and planar alignment. The frequency dependences of complex dielectric constants are very weak for both alignments. The frequency dependence is fitted using Cole-Cole equation [25] $\varepsilon^*(\omega) = \varepsilon_{\infty} + \dfrac{\varepsilon_s - \varepsilon_{\infty}}{1 + (j\omega\tau)^{1-\gamma}}$, where ε_{∞}, ε_s are "infinite frequency" and static dielectric constants, τ is the relaxation time and γ is an adjustable parameter with a value between 0 and 1. The fitted static dielectric constants obtained for the homeotropic and planar cell are used as the values of $\varepsilon_{\|}$ and $\varepsilon_{\perp}$, respectively. Static

permittivities $\varepsilon_{\|}$ and $\varepsilon_{\perp}$ are measured, at $t=-5\,°C$, Figure 5a. These data are used to plot the function $\tilde{\varepsilon}(c)$ in Figure 3b that crosses $\tilde{\sigma}(c)$ at $c=0.54$. For the mixture with $c=0.52$, the dielectric permittivities are measured over the entire range of the nematic phase, Figure 6a; these data are used to construct the monotonous dependency $\tilde{\varepsilon}(t)$ in Figure 4.

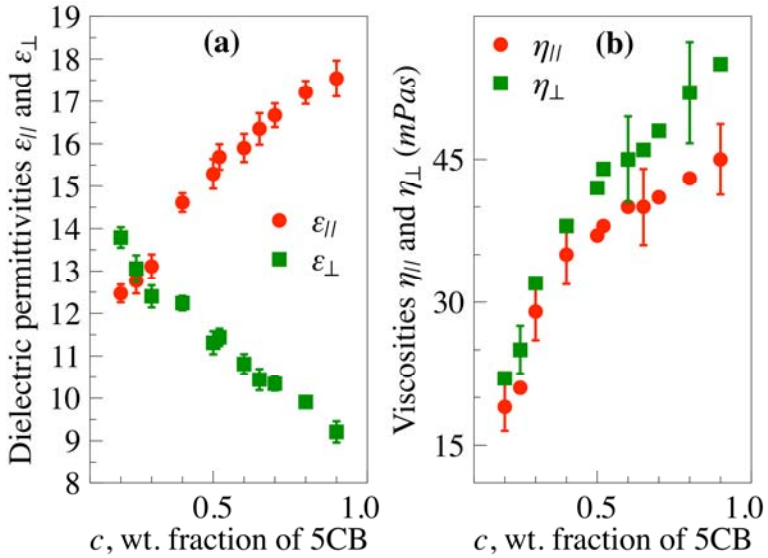

Figure 5. Concentration dependencies of dielectric permittivities and viscosity coefficients measured at $t=-5\,°C$.

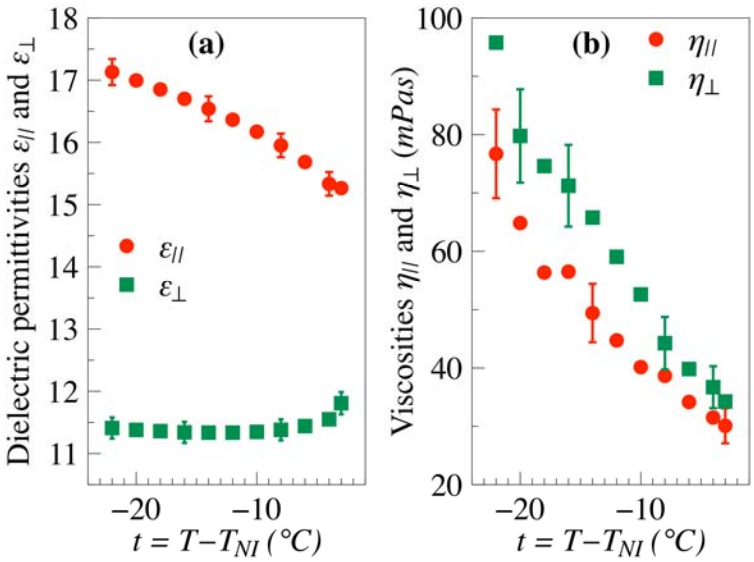

Figure 6. Temperature dependence of dielectric permittivities and viscosities of binary mixture at $c = 0.52$.

Viscosities. The effective viscosities $\eta_{\|}$ and $\eta_{\perp}$, Figs.5b and 6b, for the displacements parallel and perpendicular to $\hat{\boldsymbol{n}}_0$, respectively, [26,27] are defined from the generalized Stokes-Einstein equation $\eta_{\|,\perp} = k_B T / \left(6\pi R D_{\|,\perp}\right)$ by tracking Brownian trajectories of the same spheres as those in the electrophoretic experiments. Here k_B is the Boltzmann constant, T is the absolute temperature, $D_{\|}$ and $D_{\perp}$ are the two diffusion coefficients, measured from the time dependencies of the mean square displacements, $\left\langle \Delta x^2(\tau) \right\rangle = 2D_{\|}\tau$ and $\left\langle \Delta y^2(\tau) \right\rangle = 2D_{\perp}\tau$, respectively. The time lag τ was longer than 100 *ms* to avoid anomalous regimes [28]. Both $\eta_{\|}$ and $\eta_{\perp}$ increase with c, Figure 5b. For the mixture with $c = 0.52$, both $\eta_{\|}$ and $\eta_{\perp}$ increase as the temperature is lowered, Figure 6b.

DISCUSSION

Correlation of velocity reversals and material properties: experimental data. Comparative analysis of the dependencies $\tilde{\varepsilon}(c)$, $\tilde{\varepsilon}(t)$, $\tilde{\sigma}(c)$, $\tilde{\sigma}(t)$, $v(c)$ and $v(t)$ demonstrate a strong correlation between v and the material parameter $(\tilde{\varepsilon}-\tilde{\sigma})$, as predicted by Eq.(1). Namely, v is negative when $(\tilde{\varepsilon}-\tilde{\sigma})$ is negative and positive otherwise, Figure 3b and Figure 4. Moreover, the experimentally determined $\eta_{\|}$, $\varepsilon_{\perp}$, $\tilde{\varepsilon}$, $\tilde{\sigma}$, allowed us to fit both $v(c)$ and $v(t)$ dependencies with Eq.(1) very well, with the fitting parameter being the same within the experimental error, $\alpha = 1.1 \pm 0.2$ in Figure 3b and $\alpha = 1.2 \pm 0.2$ in Figure 4.

Equation (1) has been deduced in Ref.[9] without an explicit consideration of the exact director configuration caused by the surface anchoring at the surface of the spheres and director deformations that might be caused by the applied field through dielectric, surface polarization and flexoelectric mechanisms [29] and by viscous flow effects [30]. Below we discuss the relative importance of these distortions.

In the so-called one-constant approximation, in which all elastic constants of the liquid crystal are equal to each other and to some average value K, the field-induced realigning torques that rotate the director from the sphere-imposed direction by a small angle $\delta\theta$ can be estimated as $(K/\xi)\delta\theta$ for dielectric realignment and as $e^{*}E\delta\theta$ for the flexoelectric-surface polarization effect [29]; here K is the average Frank constant, $\xi = \sqrt{4\pi K/\Delta\varepsilon}/|E|$ is the dielectric extrapolation length, $e^{*} = e_1 + e_3 \pm P$ where e_1 and

e_3 are the flexoelectric coefficients, P is the surface polarization; e^* can be as high as [29] $e^* \sim 10^{-10}\ C/m$. For the cited electric fields, $K/\xi \sim 3\times 10^{-8}\ J/m^2$ and $e^* E \sim 2\times 10^{-6}\ J/m^2$. The latter value is not negligibly small when compared to the expected polar anchoring strength $(10^{-6} - 10^{-4})\ J/m^2$ [31-33] that is responsible for the appearance of the hedgehog next to the sphere of a diameter $2R \approx 10\ \mu m$. The Ericksen number in the problem, estimated roughly as $Er = 2\eta Rv/K$, and characterizing a ratio of the viscous to the elastic stress, is of the order of 0.1 (for $\eta = 25\ mPas$ as, $v = 2\ \mu m/s$). This value cannot be considered vanishingly small, which implies that the flow can somewhat distort the director field around the particles in our experiments. Thus both the field [29] and flow [30] might modify the director and influence α in Eq.(1). To see a stronger effect of viscous stresses, one could either use larger particles or apply a stronger electric field to increase the electrophoretic velocity. Another potential factor influencing α is the difference in dielectric permittivities of the colloid and the nematic, as it leads to gradients of the local electric field.

Correlation of velocity reversals and material properties: numerical simulations. In order to examine the correlation between the velocity and material properties, to gain a further insight into the charge distribution and flow field induced by the applied field, and to test the effect of surface anchoring on director deformation, we have developed a computational model of the transport equations [34]. We consider a 2D geometry, replacing the sphere with a disc, and neglect surface polarization and flexoelectric effects. Given the small Ericksen number, we use as input the variational

solution for the nematic field around a sphere with homeotropic anchoring [12]; we assume that the director configuration is constant. We then solve for the charge distribution and velocity fields under a uniform and oscillatory AC electric field. The particle, a disc of radius R is considered as immobilized, with a fixed location.

We use the finite element package COMSOL and consider a square domain with the side of $20R$, and a circular hole of diameter $2R = 9.6\ \mu m$ at the center, which represents the particle. We use a triangular computational mesh with 54,732 elements, which is refined near the particle and the hedgehog. We consider a fixed conductivity anisotropy, $\tilde{\sigma} = 0.4$, and solve the model for permittivity anisotropies ranging from $\tilde{\varepsilon} = -0.3$ to $\tilde{\varepsilon} = 3$. Other physical parameters are given in Table 1. The governing equations have been investigated from $t = 0$ to $t = 4\pi f$, where f is the frequency of the imposed field. We use no-slip boundary conditions for the velocity field on the edges of both the computational domain and the circular inclusion. The system is closed, so there are no flux boundary conditions for the ionic species. Finally, the electrostatic potential on two opposing boundaries is constant, with a difference given by the magnitude of the imposed field. The potential on the other two boundaries is fixed, and linearly interpolates the imposed potential difference. Of course, the potential inside the computational domains follows from the solution of Poisson's equation given the time-dependent charge distribution.

Parameter	Value	Description
$\bar{\mu}$	$1.45\times10^{-9}\ m^2/(Vs)$	Average ion mobility
$\bar{\varepsilon}$	6	Average permittivity
E_0	$19.75\ mV/\mu m$	Electric field magnitude
f	$25\ Hz$	Frequency of applied field
n_0	$10^{19}\ m^{-3}$	Average ion concentration
α_1	$-29\ mPas$	Leslie-Ericksen viscosity
α_2	$-173\ mPas$	Leslie-Ericksen viscosity
α_3	$-30\ mPas$	Leslie-Ericksen viscosity
α_4	$118\ mPas$	Leslie-Ericksen viscosity
α_5	$137\ mPas$	Leslie-Ericksen viscosity

Table 1. Parameters used in simulations of the liquid crystal-enabled electrokinetic flows.

Figure 7 shows the instantaneous charge distribution when $(\tilde{\varepsilon}-\tilde{\sigma})$ is negative (Fig. 7a) and positive (Fig. 7b), and the corresponding flow fields (averaged over a period of the field), in Fig.7c and 7d, respectively. Despite differences in the details, the resulting average flow fields for negative and positive $(\tilde{\varepsilon}-\tilde{\sigma})$ are very similar, except that the flows are completely reversed, as clear from the comparison of Fig. 6c and 6d in which the arrows indicate the velocity fields.

The electro-osmotic flows around the particle with hedgehog defect (Figure 1) acquire dipolar symmetry due to left-right asymmetry of the dipolar director configuration around the colloid, Figure 7. The asymmetry in flows causes pumping of nematic electrolyte along the x-axis, either parallel or antiparallel to the structural dipole

$\boldsymbol{p}$, depending on the sign of $(\tilde{\varepsilon}-\tilde{\sigma})$ [8,9]. In order to determine the net pumping direction near the particle, we compute the volumetric flows along the x-axis, $Q_x = \int_{-y_0}^{y_0} v_x \, dy$ and along the y-axis, $Q_y = \int_{-x_0}^{x_0} v_y \, dx$, where $x_0 = y_0 = 8R$. Under the action of the electric field, the nematic is pumped from one side of the colloid to another; there is no pumping in the orthogonal y direction, Fig. 7e and Fig. 7f. An alternative view of this pumping effect can be obtained by computing the viscous force along the x-axis on the immobile particle. The average value of this force is by integrating the normal component of the viscous stress over the surface of the particle. The dependency of this average force on $(\tilde{\varepsilon}-\tilde{\sigma})$, Fig. 8, shows a reversal of the force direction with the change of the sign of $(\tilde{\varepsilon}-\tilde{\sigma})$. When $(\tilde{\varepsilon}-\tilde{\sigma})<0$, the nematic fluid around the immobilized sphere is pumped along $\boldsymbol{p}$, Fig.7e, and the viscous force on the particle is opposite $\boldsymbol{p}$, Fig. 8. The direction $\boldsymbol{v}$ of electrophoretic propulsion of a free particle moving in the nematic with $(\tilde{\varepsilon}-\tilde{\sigma})<0$ should be in the direction opposite to the direction of the electro-osmotic pumping in Figure 7e and parallel to the direction of the viscous force calculated in Figure 8. In the experiment, the free particles in the nematic with $(\tilde{\varepsilon}-\tilde{\sigma})<0$ are indeed moving towards the negative direction of the x-axis, $v<0$, with the hedgehog leading the way, Figs. 3b, and 4. In other words, the electrophoretic velocity $\boldsymbol{v}$ is antiparallel to the dipole $\boldsymbol{p}$. For the case $(\tilde{\varepsilon}-\tilde{\sigma})>0$, polarity of electroosmotic pumping, Fig. 7f, and viscous force, Fig. 8 are reversed. This also implies that the direction of electrophoretic motion, Figs.1, 3b, 4, with respect to the structural dipole should be reversed. As seen in the experiment, when $(\tilde{\varepsilon}-\tilde{\sigma})>0$, the vectors $\boldsymbol{v}$ and

$\boldsymbol{p}$ are parallel to each other; the hyperbolic hedgehog trails the electrophoretically active sphere. Therefore, the numerical simulations confirm the experimentally determined polarity of the electrophoretic motion.

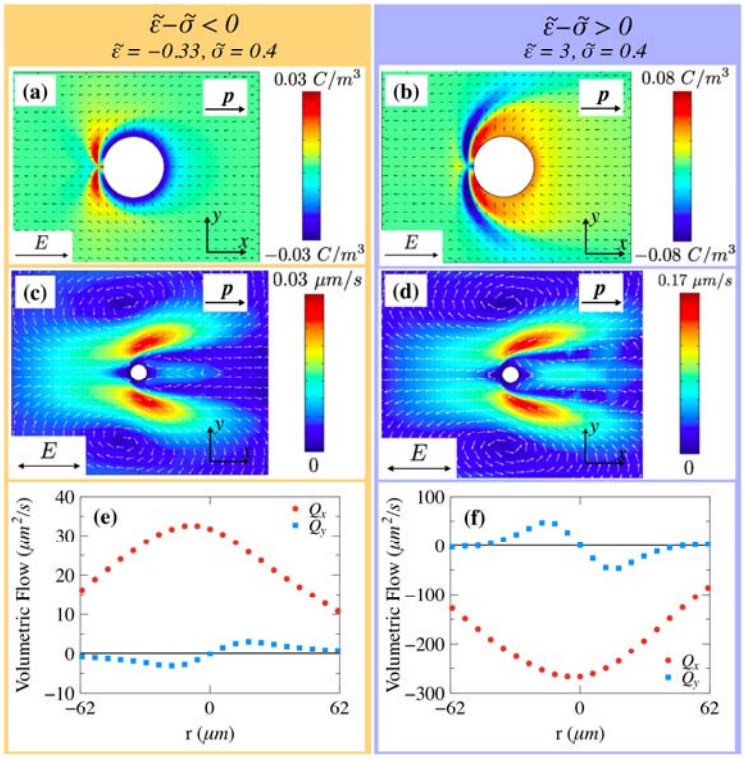

Figure 7. Numerical solutions for LCEK flows around fixed particle in two dimensions for various dielectric anisotropies, with applied field parallel to the dipole. (a)-(b) Charge density plotted in color, with arrows representing the director field. (c)-(d) Corresponding flow velocity map, showing flow reversal as $(\tilde{\varepsilon}-\tilde{\sigma})$ changes sign (e)-(f) Volumetric flows along the x-axis (Q_x) and along the y-axis (Q_y) pumped around the particle by the electric field.

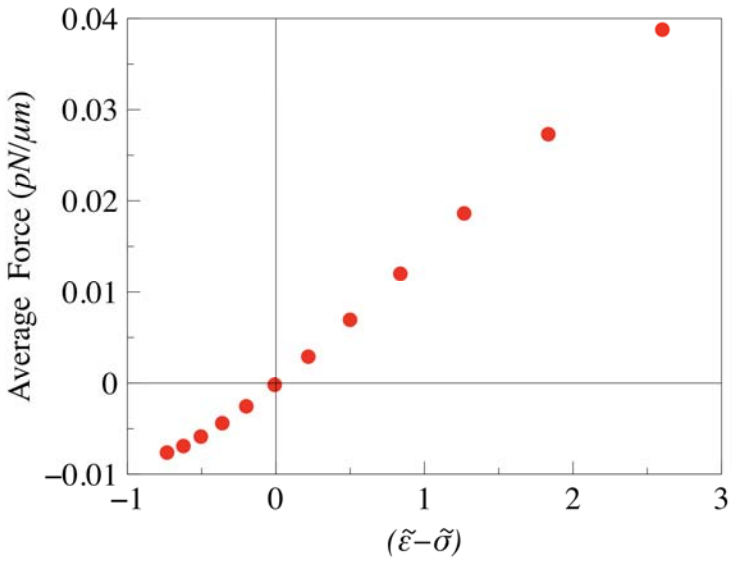

Figure 8. Average viscous force acting along the x-direction on a fixed particle by the LCEK flow, calculated for a variety of values of $(\tilde{\varepsilon}-\tilde{\sigma})$ by integrating the normal component of the viscous stress over the particle surface. Since the stress is a force per unit area, the integration yields a force per unit length. The force changes sign with $(\tilde{\varepsilon}-\tilde{\sigma})$.

CONCLUSIONS

To summarize, the measured LCEK velocities show a linear dependence on the material parameters of the nematic electrolyte, namely, the dielectric and conductivity anisotropies, as expected from the theory, Eq.(1). The experiments demonstrate that each of these two anisotropies can cause LCEK. Anisotropy of conductivity guides the ions along the pathways defined by the director, thus separating the charges in space. Dielectric anisotropy of a spatially distorted nematic acted upon by the electric field yields spatially varying local electric field; ions move in response to the nonuniform field pattern, thus creating the spatial charge. In both cases, the separated charges, acted upon by the field that created them, result in LCEK flows. Experimentally determined

electrophoretic behavior of the free spheres and numerical simulations of the immobilized spheres show a good agreement with each other. In particular, the polarities of the electrophoretic velocities of free particles are opposite to those of the electro-osmotic flows around immobilized particles.

The nematic electrolytes allow one to control both the magnitude and the polarity of electrokinetic flows by simply tuning the temperature or composition to change the value of $(\tilde{\varepsilon}-\tilde{\sigma})$.We determined the numerical coefficient in Eq.(1) that connects the electrophoretic velocity to the material parameters, as $\alpha = 1.1-1.2$. Analysis of the experimental data also suggests that the next level of detailed description of LCEK in which α is derived as a function of surface anchoring strength, flexoelectric and surface polarization effects, etc., should account for the dynamic nature of the director deformations in the applied electric field and their modification by the flows.

Acknowledgements. We acknowledge fruitful discussions with M. C. Calderer, D. Golovaty, I. Lazo-Martinez, S. Shiyanovskii, O. M. Tovkach, and N. J. Walkington. We thank J. Xiang for the help in numerical simulations. The work was supported by NSF grants DMS-1434185 (experiments on electrokinetics), DMS-1435372 and the Minnesota Supercomputing Institute (numerical simulations), as well as DMR-1410378 (determination of material parameters).

References.

[1] M. Z. Bazant, M. S. Kilic, B. D. Storey, and A. Ajdari, Towards an understanding of induced-charge electrokinetics at large applied voltages in concentrated solutions, Advances in Colloid and Interface Science **152**, 48 (2009).
[2] I. S. Aranson, Active colloids, Physics-Uspekhi **56**, 79 (2013).
[3] A. Zöttl and H. Stark, Emergent behavior in active colloids, Journal of Physics: Condensed Matter **28**, 253001 (2016).
[4] O. D. Lavrentovich, Active colloids in liquid crystals, Current Opinion in Colloid & Interface Science **21**, 97 (2016).
[5] J. Dobnikar, A. Snezhko, and A. Yethiraj, Emergent colloidal dynamics in electromagnetic fields, Soft Matter **9**, 3693 (2013).
[6] A. Ramos, *Electrokinetics and Electrohydrodynamics in Microsystems* Springer-Verlag Wien, 2011), CISM International Centre for Mechanical Sciences, 530.
[7] M. Z. Bazant and T. M. Squires, Induced-charge electrokinetic phenomena, Current Opinion in Colloid & Interface Science **15**, 203 (2010).
[8] C. Peng, Y. Guo, C. Conklin, J. Viñals, S. V. Shiyanovskii, Q.-H. Wei, and O. D. Lavrentovich, Liquid crystals with patterned molecular orientation as an electrolytic active medium, Physical Review E **92**, 052502 (2015).
[9] I. Lazo, C. Peng, J. Xiang, S. V. Shiyanovskii, and O. D. Lavrentovich, Liquid crystal-enabled electro-osmosis through spatial charge separation in distorted regions as a novel mechanism of electrokinetics, Nat Commun **5**, 5033 (2014).
[10] O. M. Tovkach, M. C. Calderer, D. Golovaty, O. Lavrentovich, and N. J. Walkington, Electro-osmosis in nematic liquid crystals, Physical Review E **94**, 012702 (2016).
[11] O. D. Lavrentovich, I. Lazo, and O. P. Pishnyak, Nonlinear electrophoresis of dielectric and metal spheres in a nematic liquid crystal, Nature **467**, 947 (2010).
[12] P. Poulin, H. Stark, T. C. Lubensky, and D. A. Weitz, Novel colloidal interactions in anisotropic fluids, Science **275**, 1770 (1997).
[13] S. Hernàndez-Navarro, P. Tierno, J. Ignés-Mullol, and F. Sagués, AC electrophoresis of microdroplets in anisotropic liquids: transport, assembling and reaction, Soft Matter **9**, 7999 (2013).
[14] S. Hernàndez-Navarro, P. Tierno, J. Ignés-Mullol, and F. Sagués, Liquid-crystal enabled electrophoresis: Scenarios for driving and reconfigurable assembling of colloids, The European Physical Journal Special Topics **224**, 1263 (2015).
[15] Y. Nishioka, F. Kobayashi, N. Sakurai, Y. Sasaki, and H. Orihara, Microscopic characterisation of self-assembled colloidal particles in electrohydrodynamic convection of a low-birefringence nematic liquid crystal, Liquid Crystals **43**, 427 (2016).
[16] I. Lazo and O. D. Lavrentovich, Liquid-crystal-enabled electrophoresis of spheres in a nematic medium with negative dielectric anisotropy, Philosophical Transactions of the Royal Society of London A: Mathematical, Physical and Engineering Sciences **371** (2013).
[17] Y. Sasaki, H. Hoshikawa, T. Seto, F. Kobayashi, V. S. R. Jampani, S. Herminghaus, C. Bahr, and H. Orihara, Direct Visualization of Spatiotemporal Structure of Self-Assembled Colloidal Particles in Electrohydrodynamic Flow of a Nematic Liquid Crystal, Langmuir **31**, 3815 (2015).
[18] S. Hernàndez-Navarro, P. Tierno, J. A. Farrera, J. Ignés-Mullol, and F. Sagués, Reconfigurable Swarms of Nematic Colloids Controlled by Photoactivated Surface Patterns, Angewandte Chemie International Edition **53**, 10696 (2014).

[19] Y. Sasaki, Y. Takikawa, V. S. R. Jampani, H. Hoshikawa, T. Seto, C. Bahr, S. Herminghaus, Y. Hidaka, and H. Orihara, Colloidal caterpillars for cargo transportation, Soft Matter **10**, 8813 (2014).
[20] J. Jadzyn and P. Kêdziora, Anisotropy of Static Electric Permittivity and Conductivity in Some Nematics and Smectics A, Molecular Crystals and Liquid Crystals **145**, 17 (1987).
[21] B.-X. Li, V. Borshch, S. V. Shiyanovskii, S.-B. Liu, and O. D. Lavrentovich, Electro-optic switching of dielectrically negative nematic through nanosecond electric modification of order parameter, Applied Physics Letters **104**, 201105 (2014).
[22] G. Vertogen and W. H. de Jeu, *Thermotropic Liquid Crystals, Fundamentals* (Springer-Verlag Berlin, 1988).
[23] K. Neyts and F. Beunis, in *Handbook of Liquid Crystals*, edited by J. W. Goodby *et al.* (Wiley-VCH Verlag GmbH & Co. KGaA, 2014), pp. 357.
[24] G. H. Heilmeier and P. M. Heyman, Note on Transient Current Measurements in Liquid Crystals and Related Systems, Physical Review Letters **18**, 583 (1967).
[25] K. S. Cole and R. H. Cole, Dispersion and Absorption in Dielectrics I. Alternating Current Characteristics, The Journal of Chemical Physics **9**, 341 (1941).
[26] J. C. Loudet, P. Hanusse, and P. Poulin, Stokes Drag on a Sphere in a Nematic Liquid Crystal, Science **306**, 1525 (2004).
[27] B. Senyuk, D. Glugla, and I. I. Smalyukh, Rotational and translational diffusion of anisotropic gold nanoparticles in liquid crystals controlled by varying surface anchoring, Physical Review E **88**, 062507 (2013).
[28] T. Turiv, I. Lazo, A. Brodin, B. I. Lev, V. Reiffenrath, V. G. Nazarenko, and O. D. Lavrentovich, Effect of Collective Molecular Reorientations on Brownian Motion of Colloids in Nematic Liquid Crystal, Science **342**, 1351 (2013).
[29] O. D. Lavrentovich, V. G. Nazarenko, V. V. Sergan, and G. Durand, Dielectric quenching of the electric polar surface instability in a nematic liquid crystal, Physical Review A **45**, R6969 (1992).
[30] J.-I. Fukuda, H. Stark, M. Yoneya, and H. Yokoyama, Dynamics of a nematic liquid crystal around a spherical particle, Journal of Physics: Condensed Matter **16**, S1957 (2004).
[31] Y. A. Nastishin, R. D. Polak, S. V. Shiyanovskii, V. H. Bodnar, and O. D. Lavrentovich, Nematic polar anchoring strength measured by electric field techniques, Journal of Applied Physics **86**, 4199 (1999).
[32] L. M. Blinov, *Structure and Properties of Liquid Crystals* (Springer Netherlands, 2011).
[33] T. Rasing and I. Muševič, *Surfaces and Interfaces of Liquid Crystals* (Springer Berlin Heidelberg, 2004).
[34] C. Conklin and J. Vinals, Electrokinetic flows in liquid crystal thin films with fixed anchoring, Soft Matter **13**, 725 (2017).